Analysis of the Simulated Climatic Characters of the South Asia High with a Flexible Coupled Ocean–Atmosphere GCM

HUANG Ying* (黄 樱) and QIAN Yongfu (钱永甫)

Department of Atmospheric Sciences, Nanjing University, Nanjing 210093

ABSTRACT

The ability of a climate model to reproduce the climatic characters of the South Asia High (SAH) is assessed by analyzing the 110-yr output of a Flexible Coupled GCM, version 0 (FGCM-0). Comparing the results of FGCM-0 with the NCEP/NCAR reanalysis data, the major findings show that FGCM-0 has better results in simulation of the geopotential height field at 100 hPa, and reproduces fairly the main atmospheric circulation centers. However, there are still some differences in the simulated results compared with the reanalysis data. The coupled model also successfully reproduces the mean seasonal variation of the SAH, that is, it moves from the Pacific Ocean to the Asian continent, remaining over the Tibetan Plateau from winter to summer, and then withdraws from the Tibetan Plateau to the Pacific Ocean from summer to winter. However, such observed relationships between the SAH positions and the summer precipitation patterns cannot be fairly reproduced in the FGCM-0.

Key words: South Asia High (SAH), FGCM-0, geopotential height, seasonal variation, SAH characteristic parameters

1. Introduction

The South Asia High (SAH) is a powerful and stable semi-permanent anticyclonic circulation pattern in the troposphere and the lower stratosphere over the Asian Continent during summer time (Mason and Anderson, 1958), and also an important part of the subtropical high pressure system. The SAH has close connections with the Northern Hemisphere summer circulation, and the Asian regional weather and climate. It can also influence the summer drought and flood patterns in China, and the weather pattern in Asia (Tao and Zhu, 1964). Many researches point out that the activities of the SAH became an important basis for weather prediction in the rainy season (Sun and Song, 1987; Luo et al., 1982; Krishnamurti et al., 1973; Zhang and Peng, 1983; Zhou, 1991). Synoptic analyses show that the ridgeline and the center of the SAH during midsummer have close relationships with the distribution of summer drought and flood in China, as it is the most important atmospheric active center in the tropopause. Many researches (Zhu et al., 1980; Sun, 1984; Liu et al., 2000; Qian, 1978; Qian et al.,

2002) find that the SAH has very obvious interannual and interdecadal variations, and also provides a strong signal of climate change in the atmosphere. On the other hand, a climate model is a powerful tool for researching the action rules of a climate system, realizing the past climatic evolution, forecasting future climatic variation, and evaluating the effects of human activities on climate change. Though nowadays the climate models are widely used in simulations and forecasts, they are improving with the advancement in understanding of the climate system. If we want to truly reproduce the climate system and forecast its future variation, we must fully utilize the actual observation data, as well as test model systems and evaluate their capability. In this way, we can find their shortcomings, and then improve them. From the developing history of numerical weather prediction, the process of test, evaluation and continuous improvement is necessary during the development of climate models (Zhou et al., 2001).

This study assesses the ability of the climate model Flexible coupled GCM version 0 (FGCM-0) to reproduce the SAH in the 100 hPa geopotential height field
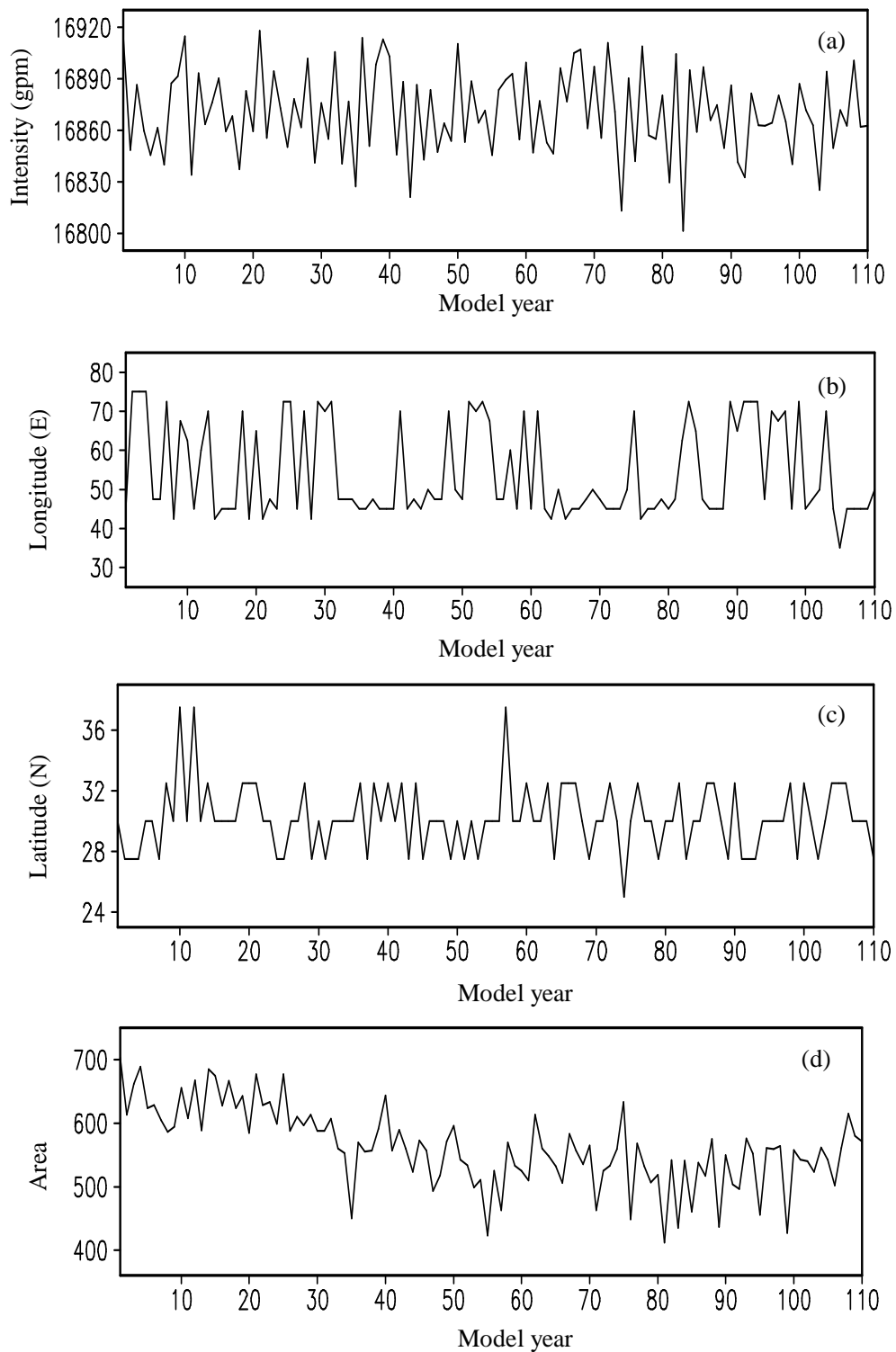
---

*E-mail: yamiao2001@yahoo.com.cn

Fig. 1. The time series of the SAH parameters in the FGCM-0: (a) the center intensity, (b) the center longitude, (c) the ridgeline, (d) the area.
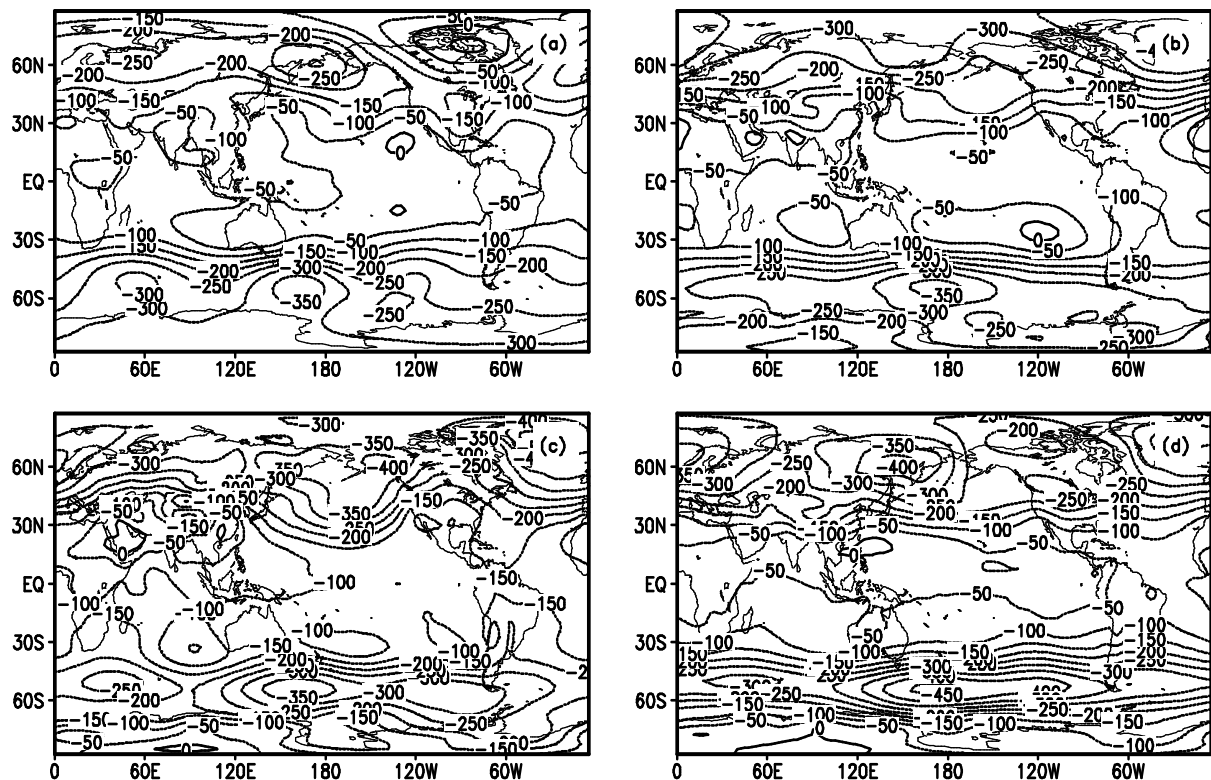
Fig. 2. The climatological difference of geopotential height at 100 hPa between the FGCM-0 simulation and the NCEP/NCAR analysis: (a) January, (b) April, (c) July, (d) October.

by analyzing its 110-yr output.

2. Introduction to the model system of the FGCM-0

In the late 1990s, the third-generation global Ocean GCM (OGCM) was developed by Jin et al. (1999) with 30 vertical layers and a grid size of about $1.875° \times 1.875°$ (T63L30). The "GM90" (Gent and McWilliams, 1990), which has a significant effect on simulating the permanent thermocline, and the "PP" scheme (Pacanowski and Philander, 1981), are also incorporated into this model. Yu et al. (2002) developed a FGCM-0, based on the National Center for Atmospheric Research (NCAR) Climate System Model version 1 (CSM-1) by replacing the CSM-1's ocean component, NCOM, with the T63L30 in virtue of the CSM's (Boville and Gent, 1998) flux coupler. The atmosphere component is the CCM3 (Kiehl et al., 1998), which is a p–σ-incorporated coordinate global model, where for the upper atmosphere the p coordinate is used, in the middle part the p–σ-incorporated coordinate is used, and in the atmosphere near the ground the σ coordinate is used. There are 18 layers in the vertical, and its horizontal grid is $2.8° \times 2.8°$. The land surface component is the Land Surface Model version

1 (LSM1), which is a one-dimensional model including energy, momentum, moisture, CO_2 transfer between the atmosphere and land, and the diversity among different vegetation types.

A simple spin-up procedure will be given as follows. Firstly, the Atmospheric General Circulation model (AGCM) (CCM3) and LSM1 are integrated for five years by using the observed climatological SST and sea ice distributions. This five-year integration is referred to as "Run 1" and the daily data from the last four years of Run 1 are archived for state variables and for radiation flux at the lowest model level. Secondly, the OGCM (T63L30) is integrated for 70 years, starting from the year 1160 of the ocean model's basic run. In this integration, the surface wind stress and thermal forcing were taken from Run 1 and this 70-yr integration is referred to as "Run 2". Following the spin-up, the fully coupled model, FGCM-0, was integrated for 60 years. The initial conditions for the atmosphere, land surface, ocean and sea ice models are taken from the end of Run 1 and Run 2, respectively (Yu et al., 2002).

The performances of FGCM-0 in simulating the climate mean states of the atmosphere, land surface, ocean, and solar radiation were evaluated. The results indicated that the FGCM-0 succeeded in controlling
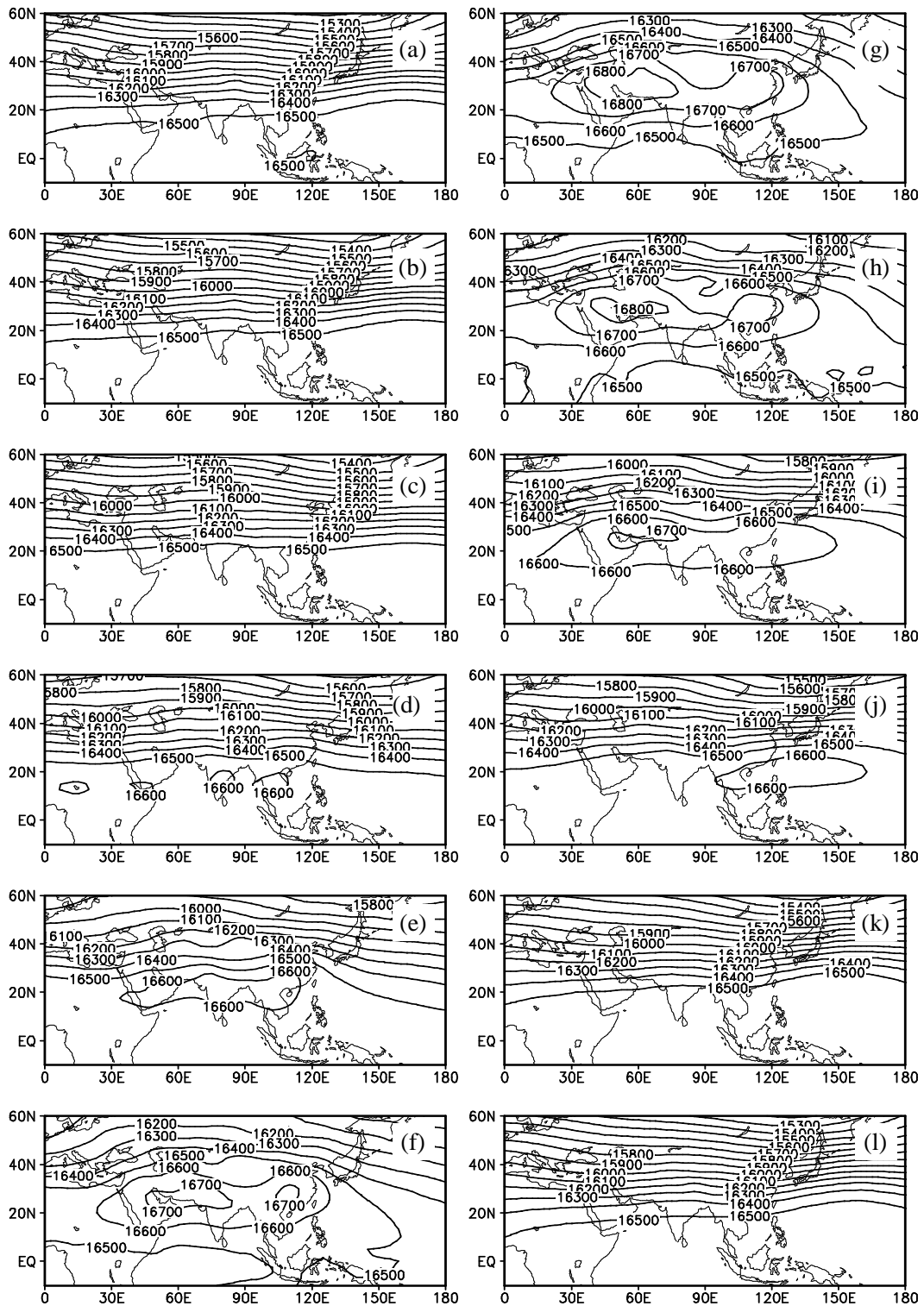
Fig. 3. The mean seasonal variation of the SAH in the FGCM-0: (a) January, (b) February, (c) March, (d) April, (e) May, (f) June, (g) July, (h) August, (i) September, (j) October, (k) November, (l) December.

the long-term climate drift and performed well in realistically reproducing the climate mean states of the atmosphere, ocean, and land surface (Yu et al., 2002; Zhang et al., 2003).

3. Definition of the SAH characteristic parameters

The Suth Asia High (SAH) characteristic parameters used in this study are the same as that defined by Zhang et al. (2000). The research domain is located in 0°–60°N, 30°W–180°E, at the 100-hPa level.

In the SAH area, the point with the largest geopotential height is defined as the center of the SAH, with the center intensity and the center longitude designated with I and L, respectively. The mean latitude of the line along which the u-component of wind is equal to zero is defined as the ridgeline of the SAH and is designated with R. The area of the SAH covers all of the grid points with a height of $\geqslant 16600$ gpm and is presented by the total point number, expressed as A.

Besides the simulated results from the FGCM-0, some observation-based data are used for assessing the simulations, including the 100-hPa geopotential height of the global NCEP/NCAR reanalysis data (Kalnay et al., 1996), and the monthly averaged precipitation at 743 stations in China.

The variations of the SAH parameters are shown in Fig. 1, which demonstrates that parameters such as the center intensity, the longitude, and the ridgeline positions of the SAH, become stable approximately 10 model years later, indicating that the position and the center geopotential height do not have a significant trend. As the area is represented by the sum of points, the area trend therefore indicates that in the first 10 years or so the number of points where the height satisfies the above condition is decreasing; only after around 40 years does the number not change any more and the area index becomes stable. Comparing with the results of Yu et al. (2002), the outputs from 11 to 110 model years are the main research period.

4. The ability of the FGCM-0 for reproducing the variation of the SAH

4.1 *Simulation of the geopotential height at 100 hPa*

There are two main atmospheric circulation systems (especially in summer) in the simulated climatological 100-hPa geopotential height field, the one over the Asian Continent being the SAH. Figure 2 shows the differences of the simulated climatological 100-hPa geopotential heights from that of the NCEP data. The figure shows that the simulated geopotential height is always lower than the reanalysis data for different seasons. The largest differences are located in the high latitudes of the Southern and Northern Hemisphere, and the smallest appear in the low latitudes. The difference in the summer half of the year is larger than in the winter half.

4.2 *Seasonal variation of the SAH in FGCM-0*

Figure 3 shows the seasonal variation of the SAH. It is well known that the SAH locates over the middle Pacific around 10°N during winter time, and its intensity is so weak that it has no obvious center (Figs. 3a, b, k, and l). The figure shows that there is no circulation center in the research area in the winter half of the year. In late April, in the Indochina peninsula, the Indian peninsula, and the east of Africa, weak centers appear that are different than the results of the reanalysis data (Fig. 3d). Then, the center of the SAH continuously shifts westward over the Indochina peninsula and its intensity increases simultaneously. In June, the center of the SAH locates over the southeast of the Tibetan Plateau in the reanalysis data and the intensity increases more obviously than in the previous months. However, the simulated results have two centers located over the southeast of the Tibetan Plateau and the Iranian Plateau, respectively (Fig. 3f). In July and August, the simulated results show that there is only a powerful center over the Iranian Plateau and the intensity of the SAH is higher in July than in August, which is just the same as that is in the NCEP data (Figs. 3g and h). From September, the SAH begins to withdraw from the Plateau. In October, both in the reanalysis data and the simulations, the center of the SAH withdraws to the Pacific (Fig. 3j). From the above discussions it is concluded that the coupled model can reproduce the seasonal variation of the SAH fairly. The movement of the SAH from the Pacific to the Asian Continent and its maintenance over the Tibetan Plateau in summer, as well as its corresponding withdrawal from the Tibetan Plateau to the Pacific, are all correctly reproduced. Figure 4 shows the seasonal variations of the SAH parameters in the NCEP/NCAR reanalysis data, the FGCM-0, and the uncoupled CCM3, respectively. Comparing with the uncoupled CCM3, the intensity in the FGCM-0 is more in accordance with the observation.

In the NCEP data, in January, the main active tropical atmospheric center is located over the middle Pacific, with its ridgeline at nearly 15°N. Simultaneously, there is also an anticyclone center over the middle of the Africa Continent. In April, there is no obvious atmospheric circulation center in the subtrop-
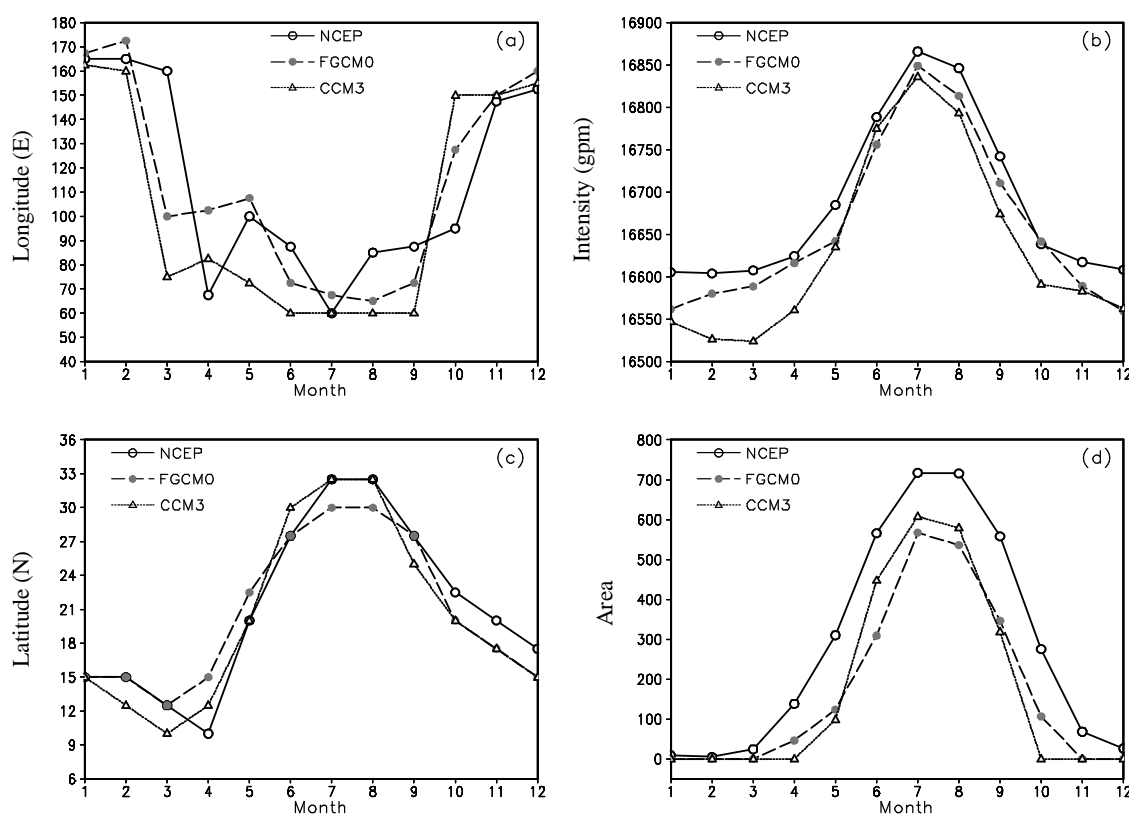
Fig. 4. The seasonal cycles of the SAH characteristic parameters: (a) Longitude of the center, (b) intensity, (c) latitude of ridgeline, (d) area.

ical areas of the Northern Hemisphere, with only some weak centers in the low latitudes. Simultaneously, the season transition of the East Asian atmospheric circulation is beginning from the winter pattern to the summer pattern. In July, there are two important atmospheric centers: the North American High (NAH), which locates over the North American continent and has its ridgeline and center at 35°N and 100°–110°W; and the SAH, which locates over the Asian continent and has its ridgeline and center at 30°N and 60°–80°E. In October, the NAH disappears and the SAH also withdraws from the continent to the ocean. Simultaneously, the atmospheric circulation moves from the summer pattern to the winter one. Figure 5 shows the simulated mean streamline field at the 100-hPa level. The main subtropical system can be found in this figure and the difference between the summer pattern and the winter pattern is remarkable. In January, the anticyclone-centers over the African continent and the middle of the Pacific are obvious. The ridgeline and the center of the anticyclone over the middle of the Pacific is more northward and eastward than that is in the reanalysis data, and the intensity of the anticyclone over the African continent is lower than in the observation data (Fig. 5a). The simulated results

in April are in accordance with the observation data (Fig. 5b). In July, the SAH ridgeline and center is located at 35°N and 60°–80°E, and the NAH is located at 38°N and 100°–110°W, and they are both more northward than that in the observation data (Fig. 5c). In October, the circulation center is located at around 20°N and 140°E; more southward, the area decreases simultaneously (Fig. 5d). From the above discussion, it is concluded that the coupled model can reproduce the main subtropical anticyclone system of the Northern Hemisphere. The centers are in accordance with the observation data, but the ridgelines are always further northward.

Figure 6 shows the seasonal variation of the ridgelines of the SAH both in the NCEP/NCAR reanalysis data, and for the simulated results. The solid lines express the ridgelines from May to October and the dashed lines from November to April. In the winter half of the year, the ridgelines of the SAH often locate around 10°N. During this time, the differences between the simulated and the observational data are not obvious. In summer, when the SAH moves to the continent, the ridges become straighter. During the seasonal variation, the ridgeline has three evident northward marches and southward withdrawals. The
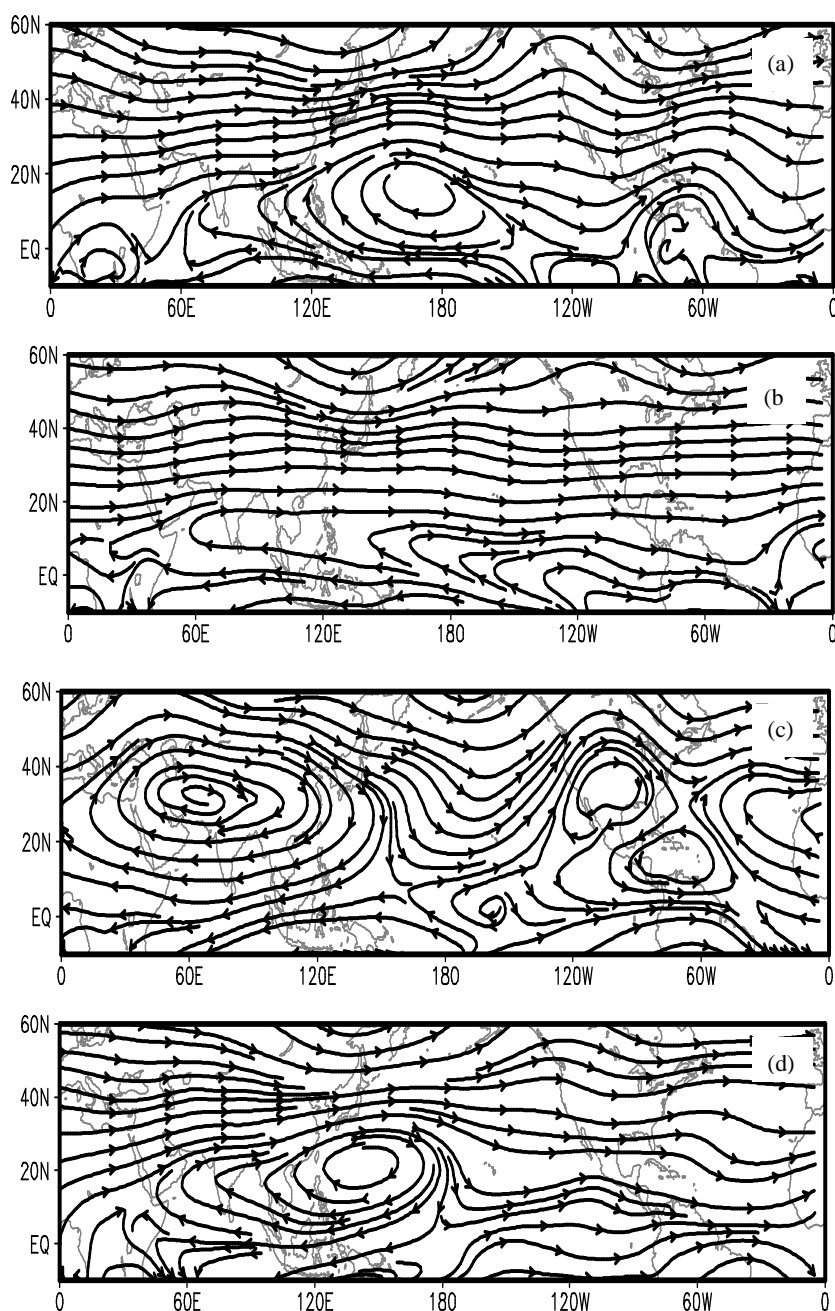
Fig. 5. The streamline field in the FGCM-0: (a) January, (b) April, (c) July, (d) October.

first northward march occurs in May, with the ridgeline moving around 20°N. The second march reaches the Yangtze River and Huaihe River area, around 25°N in June. The third march reaches the north of China, around 30°N, in July. In August, the ridgeline remains in the same location as in July. In September, it begins its first withdrawal to the location as in June. The second withdrawal occurs in October, with the ridgeline located as in May. Finally in November, the ridgeline withdraws to the ocean (Fig. 6a). Although the three northward marches and southward withdrawals can also be found in the simulated results, the average latitudes of the ridgeline during these marches and withdrawals are further southward (Fig. 6b).

The time cycle of the mean seasonal departures averaged from the equator to 50°N of the 100-hPa geopotential height is shown in Fig. 7. In the simulated results of FGCM-0, the maximum appears be-
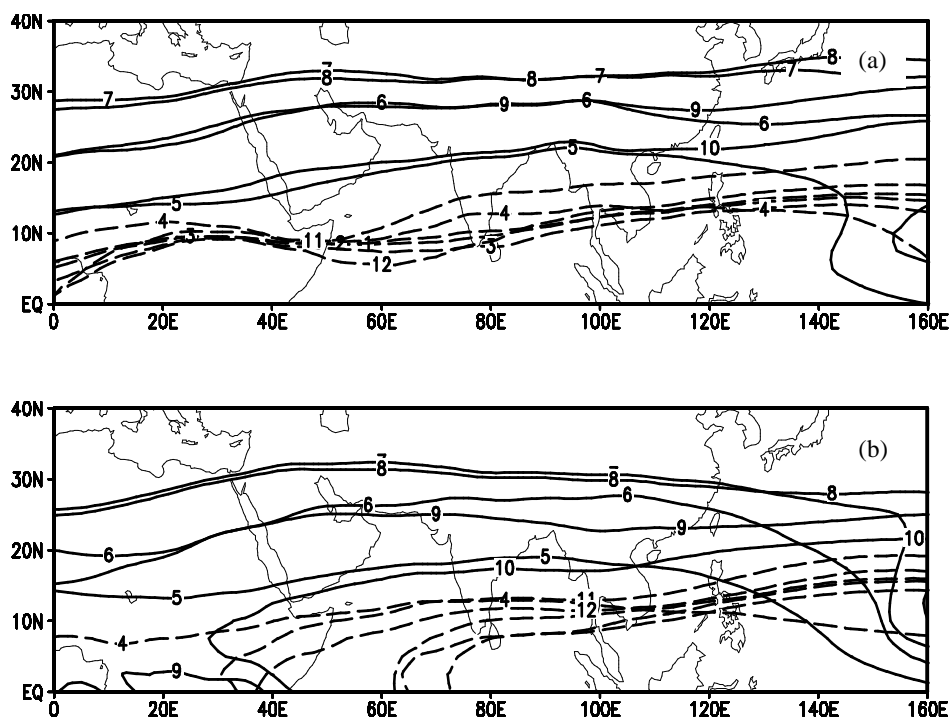
Fig. 6. The seasonal variation of the SAH ridgeline: (a) NCEP/NCAR, (b) FGCM-0.

tween July and August, and the lines whose values are equal to zero express the seasonal transition, with the first transition occurring between April and May and the second between October and November. These features are similar to those in the reanalysis data. In these two seasonal transitions, the gradient of the second transition is larger than that of the first, which implies that the second sudden change is the strongest of the two.

4.3 *Correlations between the SAH parameters*

The SAH is a semi-permanent atmospheric circulation center, and its main active period over the Asian continent is from May to September. Some studies (Zhu et al., 1980; Liu et al., 2000; Mason and Anderson, 1958; Zhang et al., 2000) indicated that the SAH has obvious interannual and interdecadal variations. After the seasonal transition in summer, the ridgeline migrates northward, and the area and the intensity increase simultaneously. This indicates that not only do parameters other than just the intensity of the SAH show seasonal variation, but also that the variation of parameters relate to each other. In order to analyze the simulated results of the SAH, the correlation coefficients between two parameters are shown in Table 1. The numbers in bold are the correlation coefficients with a statistical significance of $\geqslant 0.05$. In the NCEP/NCAR reanalysis data, the positive correlation between the parameters I and A of the SAH is very ev-

ident, showing that when the intensity increases, the area also increases (Table 1). The simulated results are able to basically reproduce the correlations of the SAH parameters (Table 2).

Table 1. The correlation coefficients of the SAH parameters in the NCEP/NCAR reanalysis data. The numbers in bold are the correlation coefficients with a statistical significance of $\geqslant 0.05$.

	May	Jun	Jul	Aug	Sep
1-L	0.08	−0.02	**−0.28**	0.02	−0.19
1-R	0.01	−0.11	**0.27**	0.01	0.12
1-A	**0.76**	**0.72**	**0.72**	**0.71**	**0.69**
L-R	−0.18	−0.18	**−0.61**	−0.21	**−0.31**
L-A	−0.01	−0.09	−0.01	0.11	0.02
R-A	**−0.28**	**−0.34**	−0.10	**−0.30**	**−0.32**

Table 2. The correlation coefficients of the SAH parameters in the FGCM-0.

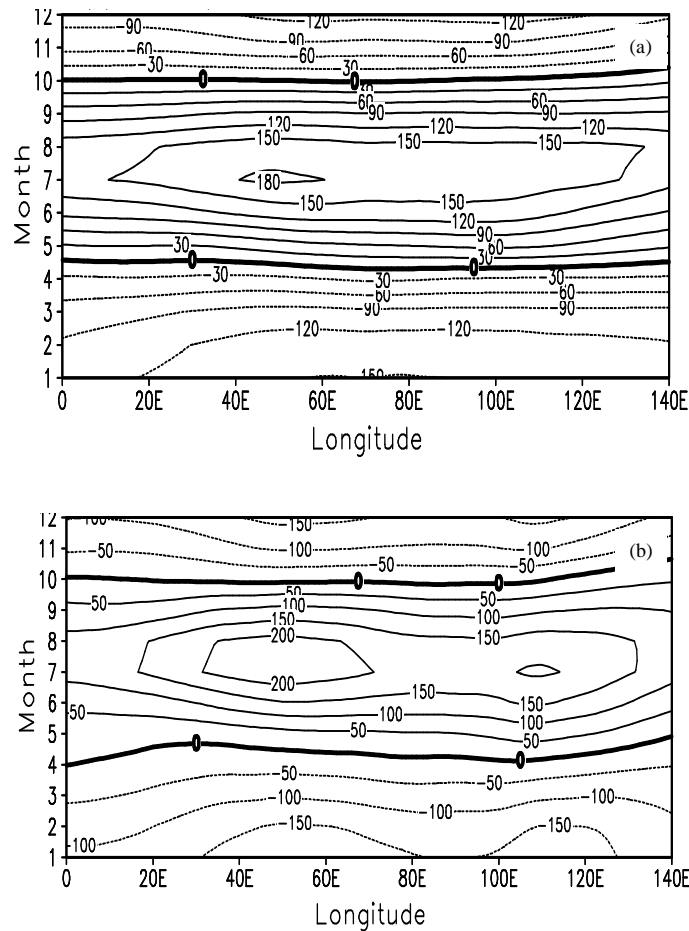|	May	Jun	Jul	Aug	Sep
1-L	0.12	−0.18	**−0.31**	−0.21	−0.01
1-R	**0.33**	**0.33**	**0.53**	**0.27**	**0.29**
1-A	**0.75**	**0.70**	**0.39**	**0.43**	**0.51**
L-R	**0.37**	**0.37**	**−0.36**	−0.18	0.02
L-A	−0.08	−0.02	−0.13	0.03	0.24
R-A	−0.11	−0.18	0.12	**−0.27**	**−0.30**

Fig. 7. The longitude-month cross section for the 100-hPa mean height departure from the Equator to 50°N: (a) NCEP/NCAR, (b) FGCM-0.

5. Relationship between the longitude location of the SAH and the summer precipitation distribution in China

Many studies have indicated that there are two balancing modes of the SAH along longitude. In summer, the longitude location of the SAH centers can be divided into two sub-modes, with one over the Iranian Plateau and the other over the Tibetan Plateau, and this east–west oscillation has certain effects on the precipitation over East Asia in summer (Tao and Zhu, 1964; Luo et al., 1982; Qian et al., 2002). As shown in Fig. 8 (observation data), the further west (east) the SAH center is, the more (less) the summer precipitation in North and South China, and the less (more) it is in the middle and lower reaches of the Yangtze River (Huang and Qian, 2003; Huang and Qian, 2004; Qian et al., 2004).

The spatial distribution of summer precipitation anomalies in the FGCM-0 for the west and east modes

are not totally realistic (Fig. 9). In the west mode, increased summer rainfall can be found in North China that is similar to the observation data, but there are differences from the observation data in so far as the summer precipitation along the Yangtze River Valley also increases, and in South China it decreases. In contrast, in the east mode, the summer precipitation decreases in North China and the Yangtze River Valley, while it increases in South China.

6. Conclusions and remarks

The coupled ocean–atmosphere GCM, version 0 (FGCM-0) has been run for 110 years without flux correction. The simulated results can reproduce fairly the distribution patterns of the main atmospheric circulation centers at the 100-hPa level, although the simulated geopotential height is lower generally than that in the reanalysis data. The model can also successfully produce the seasonal variation of the SAH, including
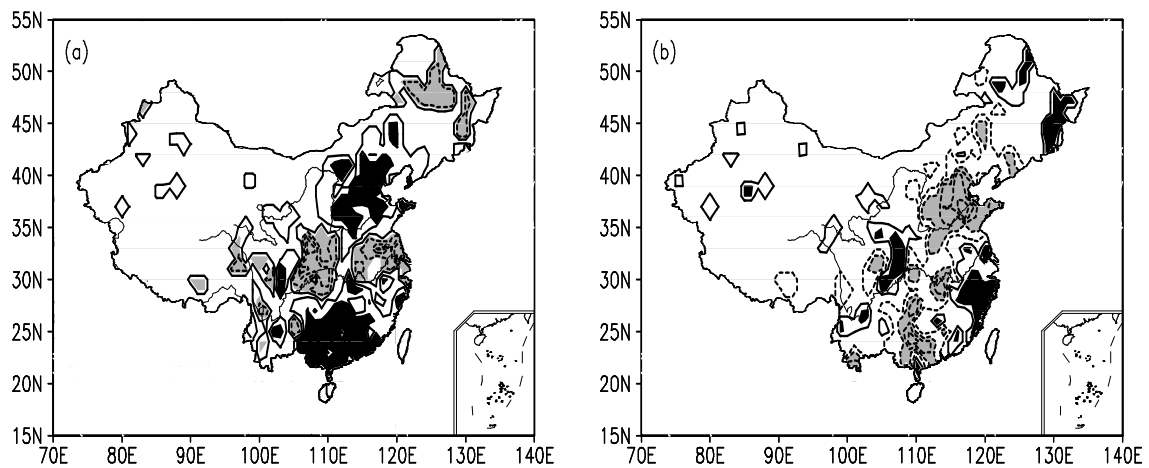
Fig. 8. Observed summer rainfall anomaly in China in the (a) west and (b) east mode (black for the positive region and gray for the negative region).
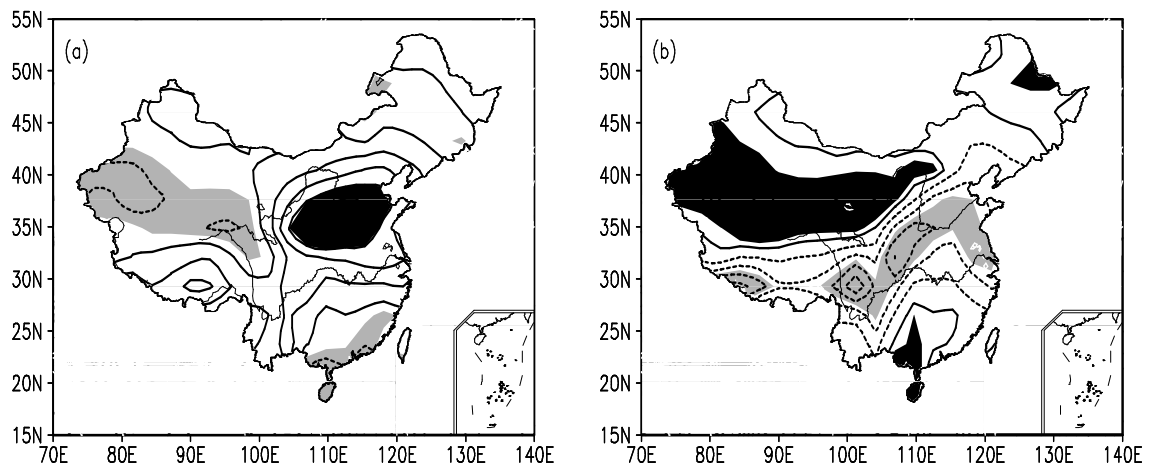

Fig. 9. Summer rainfall anomaly in China in the (a) west and (b) east mode in the FGCM-0 (black for the positive region and gray for the negative region).

the movement from the ocean to the continent during winter to summer, and its corresponding withdrawal from the Tibetan Plateau to the ocean. The simulated results in FGCM-0 are slightly better than that in the uncoupled CCM3 for the aspects of the SAH intensity and center longitude. The observed data indicates that the longitude locations of the SAH in summer exhibits two distinct modes, that is, the east mode with the SAH center located over the Tibetan Plateau, and the west mode over the Iranian Plateau; the summer precipitation distribution in China is closely associated with these two modes. However, such observed relationships between the SAH positions and the summer precipitation patterns cannot be fairly reproduced in the FGCM-0.

From the analyses in this paper, it may be concluded that the coupled models could fairly simulate the atmospheric circulations, and even their annual variations, including the semi-permanent atmospheric centers such as the SAH. Therefore, they might be used for simulations of future climatic states under the inside or outside forcing of the climate system. However, where climatic elements such as precipitation are concerned, the results from the coupled models may not be realistic and need to be carefully analyzed.

REFERENCES

Boville, B. A., and P. R. Gent, 1998: The NCAR Climate

System Model, Version One. *J. Climate*, **11**, 1115–1130.

Gent, P. R., and J. C. McWilliams, 1990: Isopycnal mixing in ocean circulation models. *J. Phys. Oceanogr.*, **20**, 150–155.

Huang Yanyan, and Qian Yongfu, 2004: Relationships between the South Asian High and characteristics of the typical droughts and floods in the mid to lower valleys of the Yangtze River and North China. *Plateau Meteorology,* **23**(1), 68–74. (in Chinese)

Huang Ying, and Qian Yongfu, 2003: The relationships between the South Asian High and summer rainfall in North China. *Plateau Meteorology,* **22**(6), 602–607. (in Chinese)

Jin Xiangze, Zhang Xuehong, and Zhou Tianjun, 1999: fundamental framework and experiments of the third generation of IAP/LASG world ocean general circulation model. *Adv. Atmos. Sci.*, **16**, 197–215.

Kalnay, E., and Coauthors, 1996: The NCEP/NCAR 40-year reanalysis project. *Bull. Amer. Meteor. Soc.,* **77**, 437–471.

Kiehl, J. T., J. J. Hack, G. B. Bonan, B. A. Boville, B. Briegleb, D. L. Williamson, and P. J. Pasch, 1998: The National Center for Atmospheric Research Community Climate Model: CCM3. *J. Climate,* **11**, 1131–1149.

Krishnamurti, T. N., S. M. Daggupaty, Jay Fein, Masao Kanamitsu, and John D. Lee, 1973: Tibetan high and upper tropospheric tropical circulations during northern summer. *Bull. Amer. Meteor. Soc.*, **54**, 1234–1249.

Liu Xuanfei, Zhu Qiangen, and Guo Pinwen, 2000: Conversion characteristics between barotropic and baroclinic circulations of the SAH and its seasonal evolution. *Adv. Atmos. Sci.*, **17**(1), 129–139.

Luo Siwei, Qian Zhengan, and Wang Qianqian, 1982: Synoptic and climatic studies on relationships between the Tibetan high and the summer floods and droughts in East China. *Plateau Meteorology*, **1**(2), 1–10. (in Chinese)

Mason, R. B., and C. E. Anderson, 1958: The development and decay of the 100mb summertime anticyclone over southern Asia. *Mon. Wea. Rev.,* **91**, 3–12.

Pacanowski, R. C., and G. Philander, 1981: Parameterization of vertical mixing in numerical models of the tropical ocean. *J. Phys. Oceanogr.*, **11**, 1442–1451.

Qian Yongfu, 1978: Computational scheme of heating fields and their effect on a process of the Tibetan High. *Papers on the Tibetan Plateau Meteorology (1975-1976),* Science Press, 199–212. (in Chinese)

Qian Yongfu, Zhang Qiong, Yao Yonghong, and Zhang Xuehong, 2002: Seasonal variation and heat preference of the South Asia High. *Adv. Atmos. Sci.*, **19,** 821–836.

Qian Yongfu, Zhang Yan, Huang Yanyan, Huang Ying and Yao Yonghong, 2004: The effects of the thermal anomalies over the Tibetan Plateau and its vicinities on climate Variability in China. *Adv. Atmos. Sci.*, **21**, 369–381.

Sun Guowu, 1984: Study on seasonal variation of the South Asia High. *Papers on the Tibetan Plateau Meteorological Experiment (Part II),* Science Press, 152–158. (in Chinese)

Sun Guowu, and Song Zhengshan, 1987: Formation of the South Asia high and its relation to circulation change and rain belt of China. *Influences of the Tibetan Plateau on the Summertime Weather in China,* Science Press, 93–100. (in Chinese)

Tao Shiyan, and Zhu Fukang, 1964: Pattern change at 100mb and its relation to advance and retreat of the subtropical Pacific High. *Acta Meteorologica Sinica*, **34**, 385–395. (in Chinese)

Yu Yongqiang, Yu Rucong, Zhang Xuehong, and Liu Hailong, 2002: A flexible global coupled climate model. *Adv. Atmos. Sci.*, **19,** 169–190.

Zhang Jijia, and Peng Yongqing, 1983: Characteristics of the South Asia High in time and frequency. *Acta Meteorologica Sinica,* **41**(3), 348–353. (in Chinese)

Zhang Qiong, Qian Yongfu, and Zhang Xuehong, 2000: Interannual and Interdecadal Variations of the South Asia High. *Chinese J. Atmos. Sci.*, **24**(1), 67–78. (in Chinese)

Zhang Xuehong, Yu Yongqiang, and Liu Hailong, 2003: The Development and Application of the Oceanic General Circulation Models Part I: The Global Oceanic General Circulation Models. *Chinese J. Atmos. Sci.*, **27**, 607–617. (in Chinese)

Zhou Jianfeng, 1991: Numerical experiments of south-north movement of the ridgeline of the South Asia high. *Acta Meteorologica Sinica,* **49**(1), 96–99. (in Chinese)

Zhou Tianjun, Yu Rucong, Zhang Xuehong, Yu Yongqiang, Li Wei, Liu Hailong, and Liu Xiying, 2001: Features of atmospheric moisture transport, convergence and air-sea freshwater flux simulated by the coupled climate models. *J. Atmos. Sci.*, **25,** 596–608. (in Chinese)

Zhu Fukang, Lu Longhua, Chen Xianji, and Zhao Wei, 1980: *The South Asia High.* Science Press, 95pp. (in Chinese)